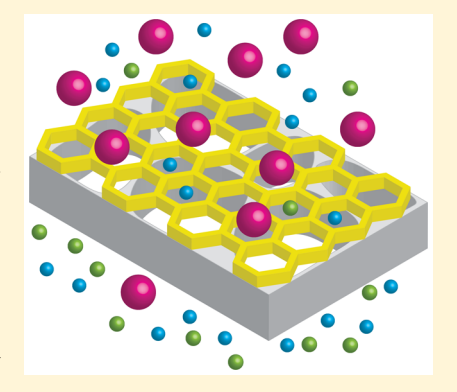


Development and Performance Characterization of a Polyimine Covalent Organic Framework Thin-Film Composite Nanofiltration Membrane

Lauren Valentino, Michio Matsumoto, William R. Dichtel, and Benito J. Mariñas J. Mariñas

Supporting Information

ABSTRACT: Two-dimensional covalent organic frameworks (COFs) were used to create the first asymmetric, thin-film composite (TFC) nanofiltration (NF) membrane with a COF active layer. NF membrane active layers of polyimine COF were synthesized via the interfacial polymerization (IP) of terephthalaldehyde and tris(4-aminophenyl)benzene monomers on top of a poly(ether sulfone) (PES) ultrafiltration membrane support. Rutherford backscattering spectrometry and Fourier transform infrared spectroscopy analyses confirmed the presence of an imine-linked film with a thickness of ~10 nm that was formed reproducibly. The rejection efficiencies of the COF NF membrane for a model organic compound, Rhodamine-WT, and a background electrolyte, NaCl, were higher than those of the PES support without the COF film. This enhanced solute rejection is the first successful demonstration of a TFC membrane with a thin COF active layer. However, this work also demonstrates the need for COF NF membranes with smaller active layer pores and alternative support materials. The former should result in greater solute rejection,



and the latter is key because the PES used for support in the COF membranes is incompatible with the organic solvents used for the COF IP process.

■ INTRODUCTION

The global demand for water is projected to increase by 55% over the next 30 years as a result of population growth, urbanization, economic development, and climate change. Inadequate sanitation in the developing world, combined with an increasing demand to reuse wastewater in developed countries, has resulted in an expanding set of contaminants that negatively impact water resources and public health. Both the need to provide safe drinking water from complex sources polluted by multiple contaminants and environmental concerns about conventional treatment methods have motivated the development of novel membrane technologies in recent decades.²⁻⁵ Nanofiltration (NF) and reverse osmosis (RO) are membrane processes commonly used for drinking water treatment because they offer an effective single-step barrier that removes both pathogens and most organic and inorganic contaminants.

For several decades, thin-film composite (TFC) membranes with polyamide (PA) active layers 50-250 nm thick have dominated the pressure-driven membrane technology sector. 6-8 These PA active layers are fabricated with interfacial polymerization (IP) reaction methods, which are advantageous because of their scalability for commercial production and capacity to produce thin (<250 nm) separating active layers with relatively high product water permeability. 6,8 However, the similarities in PA chemistry of most NF/RO membrane active layers result in a relatively limited range of water permeability and selectivity for target contaminants and background solutes. In addition, the physical, chemical, and morphological properties of the PA active layers make them susceptible to membrane compaction, fouling, and chemical degradation by oxidizing agents used to control fouling. 2-4,7,9

Given the shortcomings and limitations of current state-ofthe-art NF/RO membranes, recent efforts have focused on the development of more efficient active layer materials with enhanced water permeability, more desirable contaminant selectivity, and better fouling resistance for treating water from sources with diverse qualities. 2,4,7 Two-dimensional covalent organic frameworks (COFs) are excellent candidates for the formation of novel separating layers because they are crystalline, permanently porous, layered macromolecules with structures, chemical compositions, and porosities determined through the rational design of their monomers. 10-12 In contrast to the empirically optimized PA active layers present in current state-of-the-art NF/RO membranes, which cannot be designed

August 7, 2017 Received: Revised: November 9, 2017 Accepted: November 20, 2017 Published: November 20, 2017

[†]Safe Global Water Institute, Department of Civil and Environmental Engineering, University of Illinois at Urbana—Champaign, Urbana, Illinois 61801, United States

[‡]Department of Chemistry, Northwestern University, Evanston, Illinois 60208, United States

at the molecular level, 4 COF films can provide separating layers with uniform porosity, tailored pore size and shape, and tunable chemical functionality. 13 This potential for COF membranes is supported by molecular simulations that employed COFs as ultrathin films for desalination applications and demonstrated higher water permeability and salt rejection in comparison to PA membranes.¹⁴

COFs based on boronate ester and anhydride, 15 imine, 16 hydrazone,¹⁷ triazine,¹⁸ phenazine,¹⁹ enamine,²⁰ and imide²¹ linkages, among others, have been reported. However, they have been produced as insoluble, microcrystalline powders via solvothermal reactions. Wang et al.²² incorporated one of these preformed COF powders in a mixed-matrix PA TFC membrane to increase water permeability. Alternatively, Kandambeth et al.²³ created COF membranes by casting a thick layer of the precursors on a glass plate and heating it for 72 h. The main drawback of this approach is that the resulting membranes were $\sim 200-700 \ \mu m$ thick, lacked an asymmetric structure, and had low rejection capabilities for small organic molecules. Both the mixed-matrix TFC and thick uniform COF membranes depend on solvothermal synthesis, which clearly limit their applicability as membrane materials.

More recent efforts have focused on the development of IP reactions to form thinner imine-linked COF films. Both Dey et al.24 and Matsumoto et al.25 independently developed IP processes to form free-standing COF films, which could be transferred to various substrates to form composite membranes. The former approach produced crystalline films with approximate thicknesses of 2-5 μ m that were sandwiched between two layers of polyester fabric, and the resulting membranes rejected several aqueous solutes. In contrast, the IP method developed by Matsumoto et al.²⁵ provided precise thickness control down to 2.5 nm, and the films (~40 nm measured using AFM) exhibited high rejection of Rhodamine-WT, a small organic fluorophore. In the present study, we adapted the latter IP approach to construct the first asymmetric TFC NF membranes with thin COF active layers and comprehensively characterized the physicochemical properties and solute selectivity.

MATERIALS AND METHODS

Reagents. The COF monomer terephthalaldehyde (PDA, 99%) and solvents 1,4-dioxane (99%) and mesitylene (98%) were purchased from Sigma-Aldrich (St. Louis, MO). A catalyst, scandium(III) trifluoromethanesulfonate (Sc(OTf)₃, 98%), and the COF monomer 1,3,5-tris(4-aminophenyl)benzene (TAPB, 93%) were purchased from TCI America (Portland, OR). Permeation experiments were performed using Rhodamine-WT (R-WT; 20% w/w; Turner Designs, San Jose, CA) as a surrogate for organic contaminants and sodium chloride (NaCl; 99%; EMD Millipore, Darmstadt, Germany) as a background electrolyte. Aqueous solutions were prepared using Milli-Q water (18.2 M Ω -cm resistivity).

Active Layer Formation. COF active layers were formed via IP near the surface of an asymmetric poly(ether sulfone) (PES) ultrafiltration membrane (model HFK-328; Koch Membrane Systems, Wilmington, MA) with a molecular weight cutoff of 5000 Da. The PES support was placed in a membrane holder and secured using a silicone O-ring; both the holder and the O-ring match those used in the permeation cell described subsequently. A 1.35 mm thick aqueous layer of the catalyst was formed via the addition of 0.5 mL of 5 mM Sc(OTf)₃ over a 3.7

cm² area of the PES support encased by the O-ring to cover the PES surface completely.

Next, 0.5 mL of a second solution containing 1.56 mM TAPB monomer and 2.34 mM PDA monomer in a solvent mixture of 4:1 1,4-dioxane/mesitylene (v/v) was carefully pipetted on top of the aqueous solution as shown in Figure S1 of Supporting Information (SI). A glass cylinder with the approximate diameter of the O-ring was placed on top of the O-ring and held in place with a clamp. The open end of the cylinder was covered with a glass plate to minimize solvent evaporation (glass cylinder and plate are not shown in Figure S1 of the SI). A film was allowed to form at the interface of the two solutions for 30 min. The aqueous solution and organic solvent mixture were then suctioned through the porous PES with a syringe and needle inserted into the permeate port of the membrane holder. As a result, the polyimine COF film contacted the PES support. The resulting membrane was rinsed with methanol to remove any residual monomers, catalyst, and organic solvents. Finally, each membrane was rinsed with water under pressure (0.2 MPa) for 30 min and then used for permeation tests or air-dried for physicochemical characterization.

Physicochemical Characterization. Rutherford backscattering spectrometry (RBS) analyses were performed with a 2 MeV He⁺ beam generated by a Van de Graaff accelerator (HVE, Burlington, MA). The incident, exit, and scattering angles were 22.5°, 52.5°, and 150°, respectively. Commercial simulation software (SIMNRA; Max-Planck-Institut fur Plasmaphysik, Garching, Germany) was used for spectra fitting and analyses.

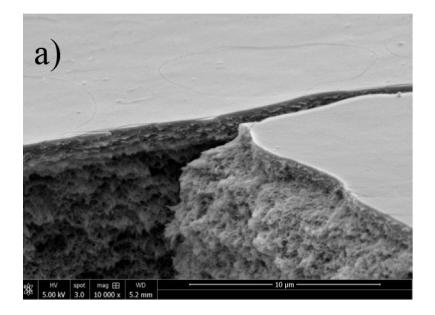
Scanning electron microscopy (SEM) was performed with a FEI Quanta 450 FEG microscope (FEI, Hillsboro, OR) to obtain high-resolution images of the membrane cross sections. Before analysis, the membranes were adhered to an aluminum puck using carbon conductive tape and sputter-coated with Au/

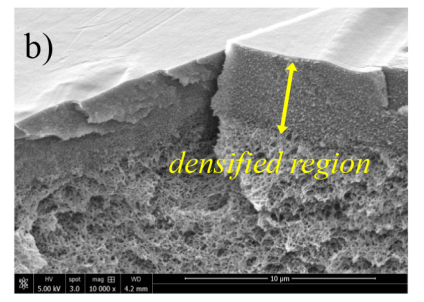
Transmission electron microscopy (TEM) was performed with a Philips CM200 TEM (FEI, Hillsboro, OR) at 120 kV. The membranes were cut into thin slices using a razor blade and embedded in an epoxy resin. After curing overnight, the epoxy blocks were sectioned using an Ultracut UCT ultramicrotome (Leica Microsystems, Buffalo Grove, IL), and the sections were collected on grids for imaging.

Fourier transform infrared (FTIR) spectra were collected using a Frontier spectrometer (PerkinElmer, Waltham, MA) equipped with a mid-infrared source, KBr beam splitter, and LiTaO₃ detector. Each spectrum, an average of 50 scans per sample, was collected at a spectral resolution of 2 cm⁻¹. A background scan was collected before the analysis and used for baseline correction.

Wide-angle X-ray scattering (WAXS) measurements were performed using a WAXS/small-angle X-ray scattering Forvis system (Forvis Technologies Inc., Santa Barbara, CA) with Cu $K-\alpha$ X-ray radiation (wavelength: 0.15418 nm) and an aerial detector (Pilatus 300 K; DECTRIS Ltd., Baden, Switzerland). The sample-to-detector distance was calibrated using a silver behenate standard before each set of measurements. The X-ray transmission patterns were processed using Fit2D (European Synchrotron Radiation Facility, Grenoble, France).

Performance Characterization. Permeation tests were conducted using a dead-end stirred cell (Amicon 8010 series, EMD Millipore, Billerica, MA) at room temperature. Feed solutions (2.5 mg/L R-WT or 400 mg/L NaCl) were adjusted **Environmental Science & Technology**





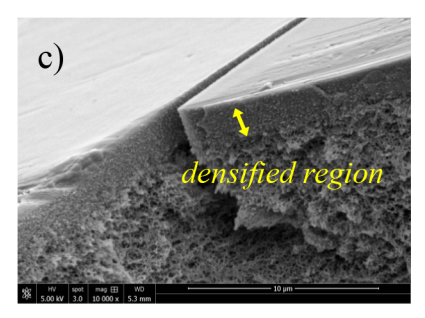


Figure 1. SEM images for cross sections of a) pristine PES membrane, b) PES+polyimine COF membrane, and c) control PES membrane at a magnification of 10 000x. Control PES membrane was exposed to organic solvents and water under the conditions used for COF film formation but in the absence of PDA, TAPB, and Sc(OTf)₂.

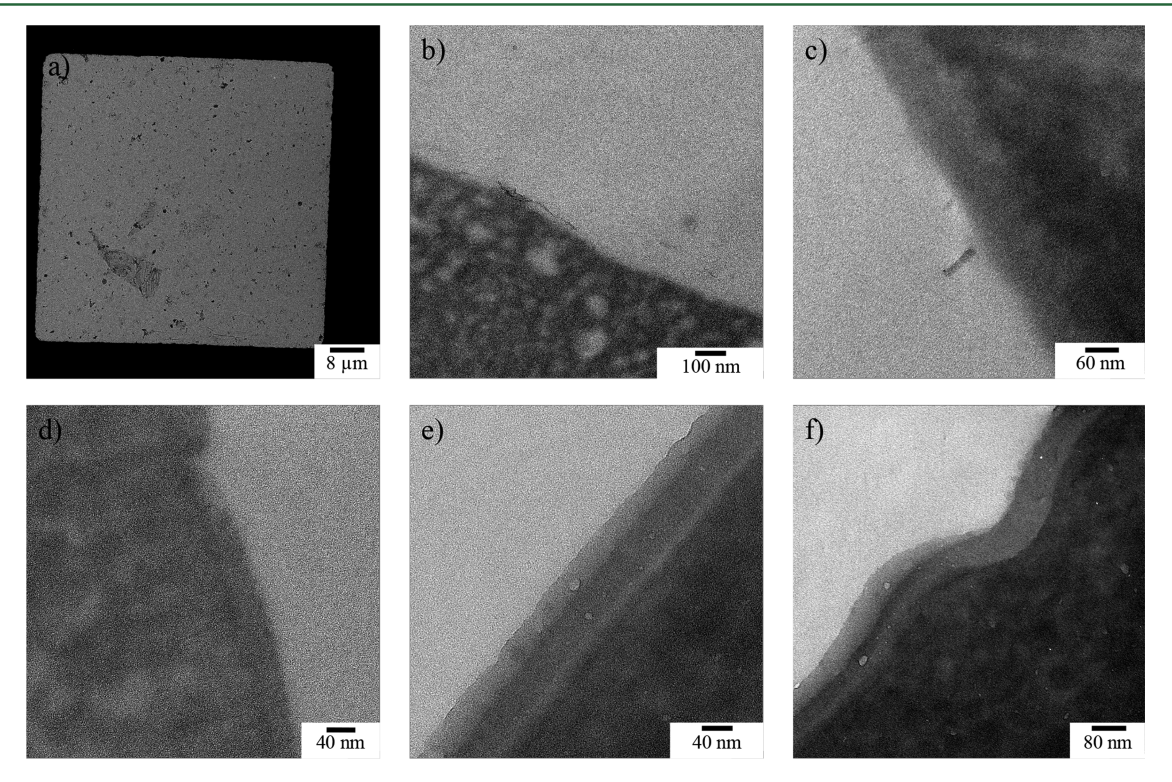


Figure 2. TEM images of a) the polyimine COF film (top view) transferred onto a TEM grid and cross sections of b) pristine PES membrane, c) PES+1 layer of the polyimine COF membrane, d) PES+3 layers of the polyimine COF membrane, and e/f) PES+6 layers of the polyimine COF membrane.

to pH 6.75 \pm 0.05 before each experiment. Permeate flow rates were measured gravimetrically using a balance, and the data were recorded using data acquisition software. Experiments were performed at several hydraulic pressures over the range of 0.01-0.5 MPa.

R-WT concentrations were measured with fluorescence using a spectrofluorometer (RF-5301PC; Shimadzu Scientific Instruments Inc., Columbia, MD) with the excitation and emission wavelengths set at 550 and 580 nm, respectively. NaCl concentrations were measured as Cl- with ion chromatography (ICS-2100; Dionex, Sunnyvale, CA). Analyses were performed with 4 mm IonPac AS18 analytical and AG18 guard columns, 23 mM KOH as the eluent, 57 mA suppressor current, a flow rate of 1 mL/min, and a 25 μ L sample loop and injection volume.

■ RESULTS AND DISCUSSION

COF Thin-Film Formation via IP. The IP reaction used to form the TAPB-PDA COF on a PES support is illustrated in Figure S1 of the SI. This reaction required several modifications in comparison to the conventional IP process used for PA active layer fabrication.^{4,7} For the COF IP, the organic phase contained both monomers, whereas the aqueous solution contained the catalyst that facilitates the reaction at the interface between the two phases. However, PES membranes are formed though a phase-inversion process in which the polymer is dissolved in a casting solution and then precipitated in a nonsolvent bath. Because of its high solubility in a variety of organic solvents, the polymer can redissolve upon contact with many solvents, ²⁶ including those used in this study. Direct exposure to the solvent mixture used for the COF IP reaction resulted in the complete dissolution of PES supports within minutes. To minimize this detrimental effect, the aqueous layer containing the catalyst acted as a protective barrier for the PES, as shown in Figure S1 of the SI.

Given the potential for the solvent to induce changes to the PES support, control experiments were performed to elucidate any effects of PES exposure to the organic solvents. These **Environmental Science & Technology**

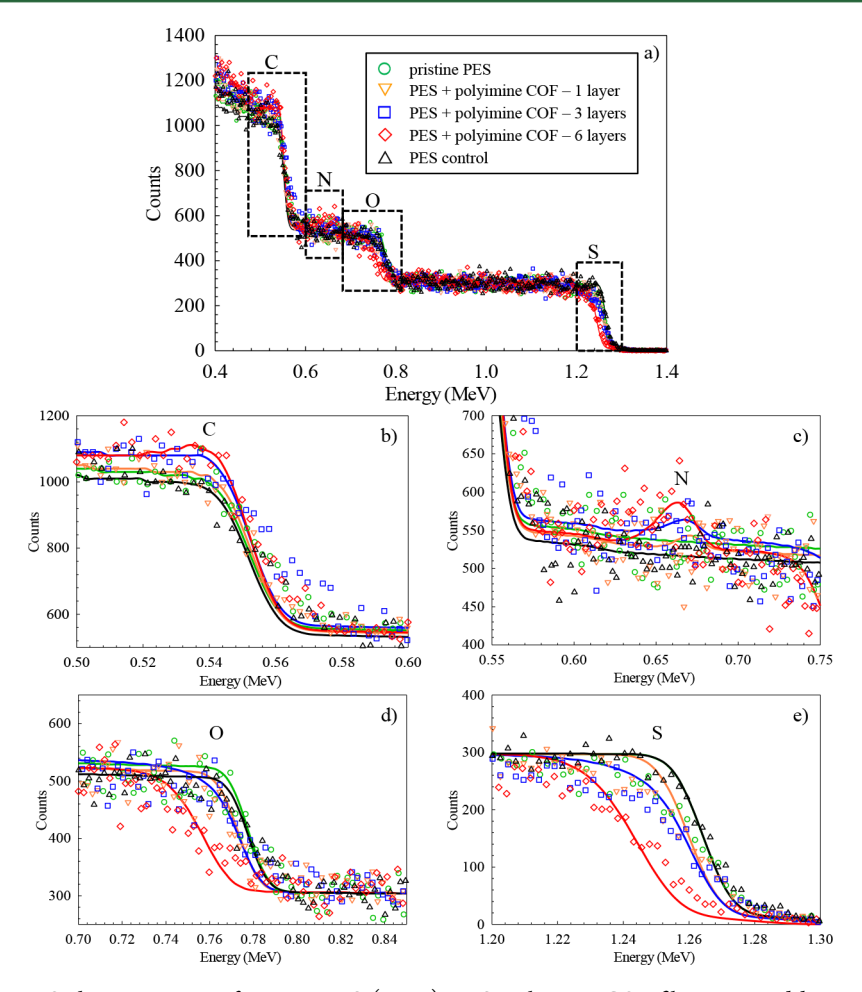


Figure 3. a) Full spectrum RBS characterization of pristine PES (green), PES+polyimine COF films prepared by performing the IP reaction 1 (orange), 3 (blue), and 6 (red) times successively, and control membrane (black). Carbon, nitrogen, oxygen, and sulfur are indicated as C, N, O, and S, respectively. Carbon b) and nitrogen c) peaks and energy offsets to oxygen d) and sulfur e) become increasingly evident as more COF layers are added. Unfilled points represent raw data points, and solid lines represent simulations obtained using SIMNRA. These simulations indicate film thicknesses of 10.4 ± 2.6 nm, 19.5 ± 3.9 nm, and 50.6 ± 3.9 nm for 1, 3, and 6 COF layers, respectively. Each thickness measurement corresponds to an average thickness measured over ~ 3 cm², and the uncertainty corresponds to the uncertainty in the RBS fitting for a single membrane sample.

control experiments exposed the PES support to water and the organic solvents under the conditions used for COF film formation but in the absence of PDA, TAPB, and Sc(OTf)₃. Without the reactants or catalyst, the control experiments did not result in COF thin film formation. However, even without direct solvent contact, the PES layer underwent the morphological changes shown in Figure 1 and Figure S2 of the SI. Exposure to the 4:1 1,4-dioxane/mesitylene solvent mixture used in the IP, with or without added TAPB and PDA monomers, resulted in a thicker, densified interfacial region within the PES. Although the aqueous layer prevented contact between the PES support and water-immiscible mesitylene, it only slowed the attack by the predominant solvent in the organic phase, 1,4-dioxane, which is miscible with water. Furthermore, contact between the PES support and the organic solvents was inevitable during the transfer of the free-standing film to the support.

TEM was used to further visually confirm film formation via the IP reaction. A TEM grid was placed at the bottom of the reactor so that the thin film was transferred directly onto the grid for analysis without rinsing to remove unreacted monomers or residual solvent. As shown in Figure 2, films that spanned the entire grid window (\sim 70 \times 70 μ m²) were

observed. The transparency indicated an extremely thin film, and visually, the film appeared intact.

Physicochemical Characterization. RBS analyses were performed on pristine PES and PES+polyimine COF membranes. As shown in Figure 3 and Figure S3 of SI, both spectra exhibited similar oxygen and sulfur plateaus despite the dense interfacial region indicated in the SEM images in Figure 1. A transformation to the elemental composition of the PES in this region would have resulted in changes to the plateau fronts (corresponding to the regions near the support surface) at ∼0.75 MeV (oxygen) and ∼1.24 MeV (sulfur). The absence of such changes confirmed that the solvent induced morphological changes without changing the chemical composition of the PES

The RBS analyses also revealed the presence of a nitrogen peak in addition to recessed sulfur and oxygen plateaus in the PES+polyimine COF membrane. These shifts to lower energy indicated losses in ion beam energy as the beam traversed into and out of the polyimine COF film before and after colliding with sulfur and oxygen atoms, which are only present in the PES support. The observed energy shifts corresponded to a COF film thickness of 10.4 ± 2.6 nm. Analyses of three additional PES+polyimine COF membrane samples confirmed that this thickness was highly reproducible. Although this

Environmental Science & Technology

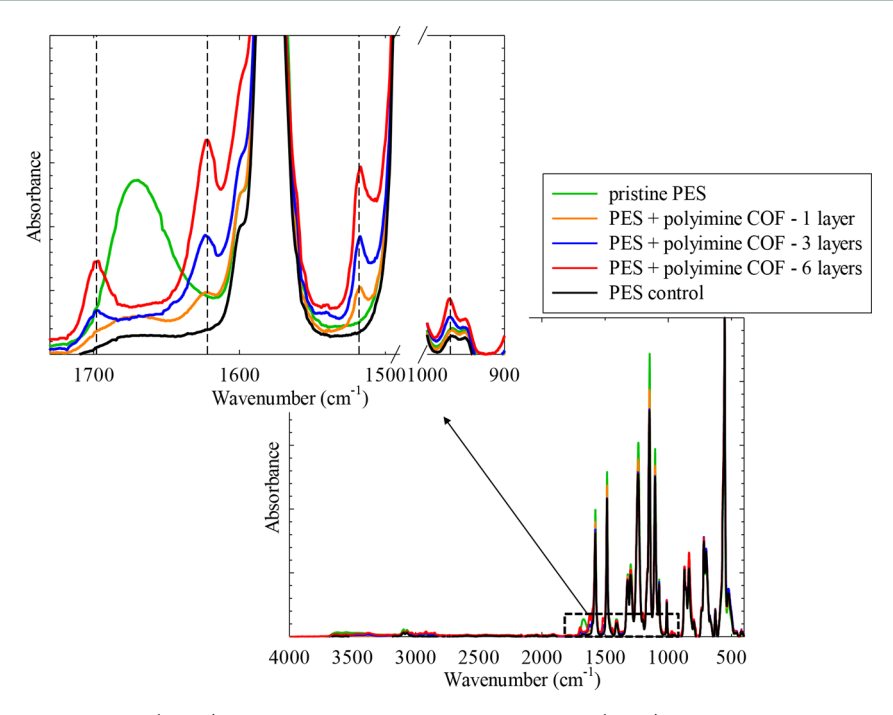


Figure 4. FTIR spectra for pristine PES (green), PES+polyimine COF, and PES control (black) membranes. The IP reaction was performed 1, 3, and 6 times consecutively to obtain 1 (orange), 3 (blue), and 6 layers (red) of the polyimine COF on top of the PES support. Vertically dashed lines in the inset indicate wavenumbers of 1698, 1622, and 970 cm⁻¹ corresponding to peaks reported in the literature for the TAPB-PDA COF, ^{30,31} while the peak at 1518 is attributed to C=C stretching of the aromatic rings. Each data set was normalized using the greatest peak intensity in that spectrum. Control PES membrane was exposed to organic solvents and water under the same conditions used for film formation but in the absence of PDA, TAPB, and Sc(OTf)₃.

measured thickness was notably thinner than that typically reported for PA membranes,⁶ it agreed relatively well with the polyimine COF thickness reported by Matsumoto et al.,²⁵ in which the COF thin film was formed under similar reaction conditions in a vial and subsequently transferred to a silicon substrate for AFM measurements.

Because RBS has a lower sensitivity for lighter elements (e.g., carbon and nitrogen, which compose the polyimine film), it is not possible to use the RBS spectrum shown in Figure S3 of the SI to ascertain the precise elemental composition of the COF active layer. Owing to this low sensitivity and the thinness of a single COF active layer, COF membranes with multiple COF layers were prepared by performing the IP reaction several times in succession. These reactions are denoted as 1, 3, and 6 layers in Figure 3. Increasing the number of layers resulted in more pronounced offsets in the sulfur and oxygen plateaus. Most important, distinct peaks for both carbon and nitrogen emerged for the membranes with 3 and 6 layers. The active layer composition, C_{0.57}H_{0.38}N_{0.05}, corresponding to the polyimine COF matched well with the experimental data (unfilled points) in Figure 3 and Figure S3 of the SI. Finally, it is notable that a scandium peak, which would appear at 1.43 MeV, was not observed in all COF membrane spectra. Due to its relatively high atomic weight of 44.96 g/mol, RBS would be more sensitive to scandium, and the absence of a peak indicates that the final rinsing step in the membrane synthesis effectively removed the catalyst to levels below detection in the COF layer and the top \sim 2 μ m of the PES support.

Cross-sectional TEM images of pristine PES and COF membranes prepared by performing the IP reaction 1, 3, and 6 times are shown in Figure 2 and revealed several notable features. Compared with those of the pristine PES, images of the COF membranes showed a distinct region of increased

thickness as the number of layers formed increased from 1 to 6. This observation supports the hypothesis that the distinct region at the surface is the COF active layer. The COF films appeared to be exceptionally smooth and contoured the underlying PES support. The thicknesses observed with TEM were greater than those determined with RBS analyses; however, compared with RBS, TEM has been shown to overestimate active layer thickness by up to 7 times.²⁸

FTIR spectra for both the TAPB and PDA monomers, PES support, powdered polyimine COF synthesized via solvothermal synthesis, ²⁹ and polyimine COF membrane are shown in Figure S4 of the SI. In contrast to the TAPB spectrum, the COF membrane spectrum showed no peaks in the primary amine region of the spectrum (3300–3500 cm⁻¹). Similarly, a band at 1685 cm⁻¹, assigned to aldehyde functional groups, was present in the PDA spectrum but absent in the COF membrane spectrum. Together, these observations confirmed the COF formation reaction and indicated that no detectable monomers were present in the membrane.

In addition to the RBS analyses, FTIR characterization was performed for COF membranes with multiple COF layers. The spectra, shown in Figure 4, revealed an intensification of the peaks at 1698, 1622, 1518, and 970 cm⁻¹ as the number of COF layers increased. The absorbance bands at 1622 cm⁻¹ (corresponding to the imine C=N stretch), 1698 cm⁻¹, and 970 cm⁻¹ have been reported for imine-linked COFs.^{30,31} The peak at 1518 cm⁻¹ was attributed to a C=C stretch in the aromatic rings.

Previously reported X-ray diffraction (XRD) analyses have confirmed that this combination of monomers produces twodimensional sheets of hexagonal-shaped pores 3.4 nm in size. ^{29,30} However, our WAXS analyses on the COF membrane were inconclusive owing to the low thickness of the active layer. ³² According to Matsumoto et al., ²⁵ it was not possible to confirm the crystallinity of the COF thin films; XRD peaks were observed only for thick films ($\sim 100~\mu m$). In an attempt to elucidate the diffraction peaks, we prepared thicker active layers by forming multiple COF layers on the PES support. Despite this effort, XRD analyses of samples with 1, 3, and 6 layers of COF yielded patterns nearly identical to those of the pristine PES, as shown in Figure S5 of the SI.

Solute Permeation. Compared with the PES support layer alone, COF active layers supported by the PES substrate provided lower water permeability and enhanced R-WT rejection, as shown in Figure 5a and Figure S6 of the SI. The

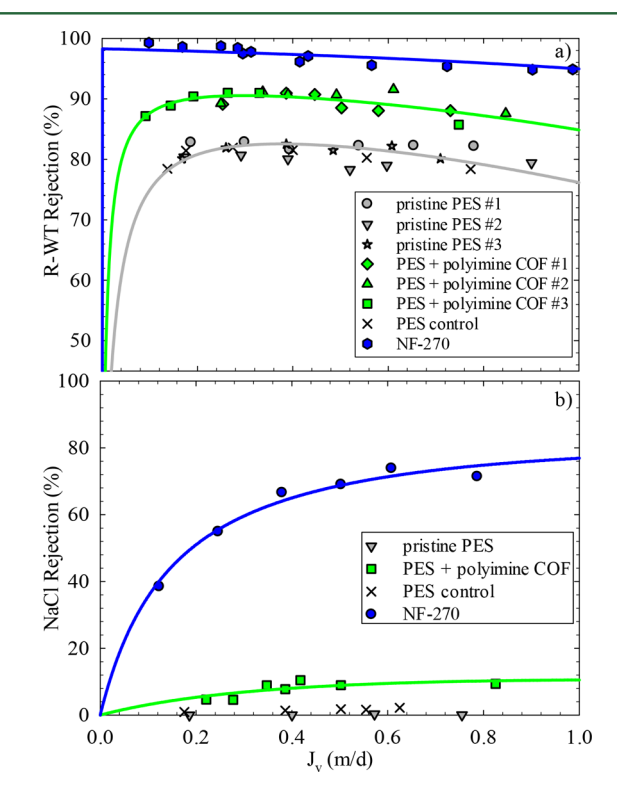


Figure 5. Rejection of (a) R-WT and (b) NaCl by pristine PES, PES +polyimine COF, control PES, and commercial NF-270 membranes. Control PES membrane was exposed to organic solvents and water under the conditions used for COF film formation but in the absence of PDA, TAPB, and Sc(OTf)₃. The permeate flux J_{ν} [m³/m²/d or m/d] is the volumetric flow rate (m³/d) normalized by the effective membrane area (m²).

three replicates demonstrated the capability of the IP reaction to produce active layers with consistent and repeatable solute selectivity even though the water permeability varied. On the basis of these independent replicates, for which permeate samples were collected after different times, the adsorption of solute was precluded as a mechanism for solute retention.

The water permeation data for each set and R-WT rejection data for all three pristine PES membranes were combined and fit with a modified solution diffusion model that accounted for advective transport through active layer imperfections. The R-WT rejection data for the three COF membrane replicates was combined and fit with a two-film solution diffusion model in order to determine the intrinsic transport parameters for the COF active layer as opposed to the composite PES-COF membrane. Detailed descriptions of the models and analysis procedure are provided in Text S1 of SI.

Table 1 shows the resulting permeation parameters: water permeation coefficient $A [m/(d \times MPa)]$, solute permeation coefficient B [m/d], and the fraction α [dimensionless] of water flux passing through membrane imperfections. The mass transfer coefficient used to represent concentration polarization of R-WT ($k_{R-WT} = 0.90 \text{ m/d}$) was calculated using the R-WT rejection data obtained for experiments performed with a Dow NF-270 semi-aromatic PA membrane. This also allowed for comparison with the performance of a state-of-the-art PA NF membrane. The water permeability and R-WT rejection data for this commercial NF membrane are also included in Figure S6 of the SI and Figure 5a, and the corresponding permeation coefficients are listed in Table 1. Despite degradation to the PES support, it is important to note that the water permeability for each of the COF membranes was greater than the water permeability for the NF-270 membrane, and this highlights the potential for TFC membranes made with thin COF active layers. Unfortunately, because most of the loss in water permeability was due to densification of the PES support, it was not possible to make a comparison per unit active layer thickness between the COF and commercial membrane.

In addition to enhanced rejection of an organic solute, the COF membranes provided measurable, although low, rejection of NaCl in contrast to the lack of rejection by the PES support, as shown in Figure 5b. The NaCl rejection data in Figure 5b correspond to the same membrane characterized before (pristine PES) and after the IP reaction (PES+polyimine COF membrane) to provide a direct comparison and evaluate the salt rejection capabilities of the COF active layer. Each solute rejection data set and the corresponding water permeability data shown in Figure S7 of the SI were fit using the procedure described in Text S1 of the SI. The resulting water and solute permeation coefficients, A and B, and α parameters are listed in Table 1. The mass transfer coefficient for NaCl $(k_{NaCl} = 2.6 \text{ m/d})$ in the concentration polarization layer was calculated from the experimentally determined value for R-WT, as described in Text S1 of the SI.

Table 1 shows that both α , which corresponds largely to membrane imperfections, and B, the solute diffusive permeation

Table 1. Water and Solute Transport Parameters Obtained by Fitting the Experimental Data in Figures 5, S6, and S7 to Equations S1, S2, S4, and S5 of SI^a

	R-WT			NaCl		
membrane	$A (m/(d\cdot MPa))$	B (m/d)	α (—)	$A (m/(d\cdot MPa))$	B (m/d)	α (—)
pristine PES	12.6 ± 0.1	0.020 ± 0.003	0.075 ± 0.006	13.0 ± 0.2	NA	NA
PES + polyimine COF	4.7 ± 0.1 , 7.6 ± 0.3 , 3.6 ± 0.1	0.012 ± 0.002	0.051 ± 0.003	3.1 ± 0.3	0.65 ± 0.51	0.76 ± 0.11
NF-270	2.9 ± 0	≤0.0005	0.016 ± 0.001	2.5 ± 0.0	0.17 ± 0.02	0.03 ± 0.04

[&]quot;Parameters B and α for R-WT and NaCl for the PES+polyimine COF membrane are listed as intrinsic transport parameters for the COF active layer.

coefficient, for the solutes R-WT and NaCl were lower for the COF membranes in comparison the PES support alone. Despite the consistent R-WT rejection capability of the COF active layers, the A parameters listed in Table 1 and corresponding to the data in Figures S6 and S7 of the SI illustrate the various losses in water permeability observed after the IP process. This result was attributed to the incompatibility between the PES support and the organic solvents used for the COF IP process as described earlier. More importantly, although the PES support damage resulted in a loss of water permeability, the rejection of R-WT and NaCl by the solvent-damaged PES layer did not increase, as shown for the control PES samples in Figure 5.

The effect of COF active layer thickness on rejection was also assessed using a membrane for which the IP reaction was performed twice sequentially, and the resulting two layers were considered to form a single film on the PES support. These layers were analyzed with the two-film model for solute permeation. Given that the solute permeation coefficient B is inversely proportional to thickness, a thicker active layer is expected to provide a greater barrier to diffusive solute transport, which corresponds to higher rejection in the low pressure/flux regime. The ratio of thicknesses (1 layer = 10.4 nm, 2 layers = 16.9 nm) was used to calculate $B_{COF2} = 0.007 \text{ m/}$ d, assuming that α_{COF2} remains 0.051. These parameters were used to predict the rejection behavior for the COF membrane prepared by performing the IP reaction twice. As shown in Figure S8 of the SI, the predicted simulation agreed relatively well with the experimental data within the range of variability observed. The model and experimental data also confirmed that the rejection properties of the active layer did not change significantly when the membrane thickness increased by ~62%.

Finally, as shown in Figure S6 of the SI, the decrease in water permeability for this membrane was greater due to the damage incurred to the PES support as a result of prolonged exposure to degrading solvents. Owing to this severe damage, we could not test thicker COF active layers.

Relevance and Potential. We successfully prepared a TFC membrane with a polyimine COF active layer. Although its performance was not optimal in terms of water permeability and solute rejection, the membrane represents a new generation of NF membranes with active layers that are controllable at the molecular level. The focus of this study was to use a two-dimensional COF (pore size ~3.4 nm)²⁵ synthesized with triamine and dialdehyde monomers, but pore size can be modulated by varying the combination of monomers. Postsynthetic modifications offer additional opportunities for external surface and inner-pore functionalization and the tuning of chemical properties. For example, Waller et al.³¹ recently described the conversion of the imine linkages into amide linkages using an oxidative process in a TAPB-PDA COF. Currently, the limit to expanding the library of COF membranes is the solvent support compatibility issue. However, this limitation can be overcome by leveraging solvent-resistant support materials, such as those used for organic solvent filtration.²⁶ Finally, although no delamination was observed with COFs produced from the combination of TAPB and PDA monomers, adhesion between the COF active layer and underlying support may play an important role in the longterm performance of TFC membranes consisting of COF active layers and should be the focus of further studies. Overall, the combination of solvent-resistant supports with modified COF structures offers a new paradigm for NF/RO membrane design

in which membrane properties are rationally tunable at the molecular level.

ASSOCIATED CONTENT

S Supporting Information

The Supporting Information is available free of charge on the ACS Publications website at DOI: 10.1021/acs.est.7b04056.

Figure S1, schematic of the IP reaction and synthesis of imine-linked two-dimensional COF; Figure S2, SEM images for cross sections of pristine PES, COF, and control membranes; Figure S3, RBS spectra for pristine PES and COF membranes; Figure S4, FTIR spectra of TAPB and PDA monomers, polyimine COF powder, COF membrane, and pristine PES; Figure S5, WAXS diffractograms for the pristine PES and COF membranes; Figure S6, water permeability data for the R-WT experiments; Figure S7, water permeability data for the NaCl experiments; equations S1 and S2, which were used to fit data for water flux and permeation with the singlefilm model; equation S3, which was used to calculate the mass transfer coefficients for NaCl; equations S4, S5, and S6, which were used to fit data for R-WT permeation with the two-film model; Figure S8, R-WT rejection for COF membrane with two layers; and additional references (PDF)

AUTHOR INFORMATION

Corresponding Author

*Phone: +1-217-333-6961; e-mail: marinas@illinois.edu (B.J.M.).

ORCID ®

Michio Matsumoto: 0000-0002-6037-0228 William R. Dichtel: 0000-0002-3635-6119 Benito J. Mariñas: 0000-0002-8485-2037

Notes

The authors declare no competing financial interest.

ACKNOWLEDGMENTS

RBS and XRD analyses were carried out in the Frederick Seitz Materials Research Laboratory Central Facilities at the University of Illinois. SEM and TEM analyses were performed at the Beckman Institute at the University of Illinois. We thank Mauro Sardela and Scott Robinson for assistance with XRD and SEM/TEM, respectively. This material is based upon work supported by the National Science Foundation under Grant No. 1706219 and the Army Research Office through the Multidisciplinary University Research Initiative (MURI, W911NF-15-1-0447, to W.R.D.). The opinions of this paper do not necessarily reflect those of the sponsors.

REFERENCES

- (1) WWAP The United Nations World Water Development Report 2015: Water for a Sustainable World; UNESCO: Paris, 2015.
- (2) Lee, K. P.; Arnot, T. C.; Mattia, D. A Review of Reverse Osmosis Membrane Materials for Desalination—Development to Date and Future Potential. *J. Membr. Sci.* **2011**, 370 (1–2), 1–22.
- (3) Pendergast, M. M.; Hoek, E. M. V. A Review of Water Treatment Membrane Nanotechnologies. *Energy Environ. Sci.* **2011**, *4* (6), 1946–1971
- (4) Werber, J. R.; Osuji, C. O.; Elimelech, M. Materials for Next-Generation Desalination and Water Purification Membranes. *Nat. Rev. Mater.* **2016**, *1* (5), 16018.

- (5) Shannon, M. A.; Bohn, P. W.; Elimelech, M.; Georgiadis, J. G.; Marinas, B. J.; Mayes, A. M. Science and Technology for Water Purification in the Coming Decades. *Nature* **2008**, *452* (7185), 301–310
- (6) Petersen, R. J. Composite Reverse Osmosis and Nanofiltration Membranes. *J. Membr. Sci.* **1993**, *83* (1), 81–150.
- (7) Elimelech, M.; Phillip, W. A. The Future of Seawater Desalination: Energy, Technology, and the Environment. *Science* **2011**, 333 (6043), 712–717.
- (8) Cadotte, J. E.; Petersen, R. J. Thin-Film Composite Reverse-Osmosis Membranes: Origin. ACS Symposium 1981, 153, 305–326.
- (9) Baker, R. W. Membrane Technology and Applications, 2nd ed.; John Wiley & Sons, Ltd: New York, 2004.
- (10) Feng, X.; Ding, X.; Jiang, D. Covalent Organic Frameworks. Chem. Soc. Rev. 2012, 41 (18), 6010–6022.
- (11) Ding, S. Y.; Wang, W. Covalent Organic Frameworks (COFs): From Design to Applications. *Chem. Soc. Rev.* **2013**, 42 (2), 548–568.
- (12) Waller, P. J.; Gándara, F.; Yaghi, O. M. Chemistry of Covalent Organic Frameworks. Acc. Chem. Res. 2015, 48 (12), 3053–3063.
- (13) Bisbey, R. P.; Dichtel, W. R. Covalent Organic Frameworks as a Platform for Multidimensional Polymerization. *ACS Cent. Sci.* **2017**, *3* (6), 533–543.
- (14) Lin, L.-C.; Choi, J.; Grossman, J. C. Two-Dimensional Covalent Triazine Framework as an Ultrathin-Film Nanoporous Membrane for Desalination. *Chem. Commun.* **2015**, *51* (80), 14921–14924.
- (15) Côté, A. P.; Benin, A. I.; Ockwig, N. W.; O'Keeffe, M.; Matzger, A. J.; Yaghi, O. M. Porous, Crystalline, Covalent Organic Frameworks. *Science* **2005**, *310* (5751), 1166–1170.
- (16) Uribe-Romo, F. J.; Hunt, J. R.; Furukawa, H.; Klöck, C.; O'Keeffe, M.; Yaghi, O. M. A Crystalline Imine-Linked 3-D Porous Covalent Organic Framework. *J. Am. Chem. Soc.* **2009**, *131* (13), 4570–4571.
- (17) Uribe-Romo, F. J.; Doonan, C. J.; Furukawa, H.; Oisaki, K.; Yaghi, O. M. Crystalline Covalent Organic Frameworks with Hydrazone Linkages. *J. Am. Chem. Soc.* **2011**, *133* (30), 11478–11481.
- (18) Kuhn, P.; Antonietti, M.; Thomas, A. Porous, Covalent Triazine-Based Frameworks Prepared by Ionothermal Synthesis. *Angew. Chem., Int. Ed.* **2008**, *47* (18), 3450–3453.
- (19) Guo, J.; Xu, Y.; Jin, S.; Chen, L.; Kaji, T.; Honsho, Y.; Addicoat, M. A.; Kim, J.; Saeki, A.; Ihee, H.; Seki, S.; Irle, S.; Hiramoto, M.; Gao, J.; Jiang, D. Conjugated Organic Framework with Three-Dimensionally Ordered Stable Structure and Delocalized Pi Clouds. *Nat. Commun.* 2013, 4, 2736.
- (20) Kandambeth, S.; Mallick, A.; Lukose, B.; Mane, M. V.; Heine, T.; Banerjee, R. Construction of Crystalline 2D Covalent Organic Frameworks with Remarkable Chemical (Acid/Base) Stability Via a Combined Reversible and Irreversible Route. *J. Am. Chem. Soc.* **2012**, 134 (48), 19524–19527.
- (21) Fang, Q.; Zhuang, Z.; Gu, S.; Kaspar, R. B.; Zheng, J.; Wang, J.; Qiu, S.; Yan, Y. Designed Synthesis of Large-Pore Crystalline Polyimide Covalent Organic Frameworks. *Nat. Commun.* **2014**, *5*, 4503.
- (22) Wang, C.; Li, Z.; Chen, J.; Li, Z.; Yin, Y.; Cao, L.; Zhong, Y.; Wu, H. Covalent Organic Framework Modified Polyamide Nano-filtration Membrane with Enhanced Performance for Desalination. *J. Membr. Sci.* **2017**, 523, 273–281.
- (23) Kandambeth, S.; Biswal, B. P.; Chaudhari, H. D.; Rout, K. C.; Kunjattu, H. S.; Mitra, S.; Karak, S.; Das, A.; Mukherjee, R.; Kharul, U. K.; Banerjee, R. Selective Molecular Sieving in Self-Standing Porous Covalent-Organic-Framework Membranes. *Adv. Mater.* **2017**, 29 (2), 1603945.
- (24) Dey, K.; Pal, M.; Rout, K. C.; Kunjattu, H. S.; Das, A.; Mukherjee, R.; Kharul, U. K.; Banerjee, R. Selective Molecular Separation by Interfacially Crystallized Covalent Organic Framework Thin Films. J. Am. Chem. Soc. 2017, 139 (37), 13083–13091.
- (25) Matsumoto, M.; Valentino, L.; Stiel, G. M.; Balch, H. B.; Corcos, A. R.; Wang, F.; Ralph, D. C.; Marinas, B. J.; Dichtel, W. R. Lewis Acid-Catalyzed Interfacial Polymerization of Covalent Organic

- Framework Films and Their Integration into Nanofiltration Membranes. *Chem* **2017**, in press.
- (26) Marchetti, P.; Jimenez Solomon, M. F.; Szekely, G.; Livingston, A. G. Molecular Separation with Organic Solvent Nanofiltration: A Critical Review. *Chem. Rev.* **2014**, *114* (21), 10735–10806.
- (27) Mi, B.; Coronell, O.; Marinas, B.; Watanabe, F.; Cahill, D.; Petrov, I. Physico-Chemical Characterization of NF/RO Membrane O Active Layers by Rutherford Backscattering Spectrometry. *J. Membr. Sci.* **2006**, 282 (1–2), 71–81.
- (28) Lin, L.; Feng, C.; Lopez, R.; Coronell, O. Identifying Facile and Accurate Methods to Measure the Thickness of the Active Layers of Thin-Film Composite Membranes a Comparison of Seven Characterization Techniques. *J. Membr. Sci.* **2016**, *498*, 167–179.
- (29) Matsumoto, M.; Dasari, R. R.; Ji, W.; Feriante, C. H.; Parker, T. C.; Marder, S. R.; Dichtel, W. R. Rapid, Low Temperature Formation of Imine-Linked Covalent Organic Frameworks Catalyzed by Metal Triflates. *J. Am. Chem. Soc.* **2017**, *139* (14), 4999–5002.
- (30) Smith, B. J.; Overholts, A. C.; Hwang, N.; Dichtel, W. R. Insight into the Crystallization of Amorphous Imine-Linked Polymer Networks to 2D Covalent Organic Frameworks. *Chem. Commun.* **2016**, 52 (18), 3690–3693.
- (31) Waller, P. J.; Lyle, S. J.; Osborn Popp, T. M.; Diercks, C. S.; Reimer, J. A.; Yaghi, O. M. Chemical Conversion of Linkages in Covalent Organic Frameworks. *J. Am. Chem. Soc.* **2016**, *138* (48), 15519–15522.
- (32) Hexemer, A.; Müller-Buschbaum, P. Advanced Grazing-Incidence Techniques for Modern Soft-Matter Materials Analysis. *IUCrJ* **2015**, 2 (1), 106–125.
- (33) Urama, R. I.; Mariñas, B. J. Mechanistic Interpretation of Solute Permeation through a Fully Aromatic Polyamide Reverse Osmosis Membrane. *J. Membr. Sci.* **1997**, *123* (2), 267–280.